

Geometric Optimal Control of Mechanical Systems with Gravitational and Resistive Force

Jinwoo Choi, Alejandro Cabrera, and Ross L. Hatton

Abstract—Optimal control plays a crucial role in numerous mechanical and robotic applications. Broadly, optimal control methods are divided into direct methods (which optimize trajectories directly via discretization) and indirect methods (which transform optimality conditions into equations that guarantee optimal trajectories). While direct methods could mask geometric insights into system dynamics due to discretization, indirect methods offer a deeper understanding of the system’s geometry. In this paper, we propose a geometric framework for understanding optimal control in mechanical systems, focusing on the combined effects of inertia, drag, and gravitational forces. By modeling mechanical systems as configuration manifolds equipped with kinetic and drag metrics, alongside a potential field, we explore how these factors influence trajectory optimization. We derive optimal control equations incorporating these effects and apply them to two-link and UR5 robotic manipulators, demonstrating how manifold curvature and resistive forces shape optimal trajectories. This work offers a comprehensive geometric approach to optimal control, with broad applications to robotic systems.

I. INTRODUCTION

The optimal control has a long and rich history, from the Brachistochrone curve to various applications in robotics, such as manipulators, legged locomotion systems [1], [2], [3], and undulatory locomotion systems [4], [5], [6]. Optimal control methods can generally be categorized into two main approaches: *direct* and *indirect* methods.

Direct methods involve discretizing trajectories and using the waypoint locations (or other parameterization) as decision variables to solve the optimal control problem directly. Although this approach is relatively straightforward to implement, it can obscure the geometric properties of the problem. In contrast, indirect methods employ the *Pontryagin Maximum Principle* to transform the optimal control problem into a differential equation. Then, a problem structure of the optimal control can be seen as a boundary value problem, which can be solved via a shooting method.¹ These differential equations often offer deeper geometric insights into the optimal trajectories. For this paper, we focus on geometric optimal control, which primarily focuses on indirect methods.

In Lagrangian mechanics, the mechanical systems can be expressed in terms of a *Riemannian manifold* associated with

Jinwoo Choi and Ross L. Hatton are with the Collaborative Robotics and Intelligent Systems (CoRIS) Institute at Oregon State University, Corvallis, OR USA. {choijinw, Ross.Hatton}@oregonstate.edu

Alejandro Cabrera is with Instituto de Matemática, Universidade Federal do Rio de Janeiro, Rio de Janeiro, Brazil. alejandro@matematica.ufrj.br

¹This method can be implemented by these steps: 1) fix some initial conditions, 2) iterate over high-order initial conditions while shooting guaranteed-optimal trajectories to hit low-order final conditions.

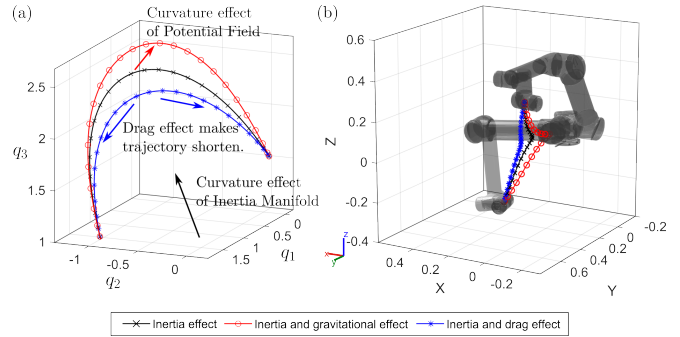


Fig. 1. (a) Optimal trajectories for a UR5 moving its first three joints. The black- \times -marked curve denotes the optimal trajectory considering only the inertia effect. The distortion based on the curvature of the inertia manifolds adds acceleration to the trajectory in the direction to reduce the inertia effect (e.g., the configuration folding the arm). The red- o -marked curve includes both inertia and gravitational effects, influenced by the curvature of the potential field on the inertia manifold. The blue curve denotes the optimal trajectory considering both inertia and drag, where drag force is modeled as a joint viscous friction. In this case, a drag metric reduces to an Euclidean metric, shortening the optimal trajectory in configuration space. (b) The same optimal trajectories in task space as those in configuration space with the initial and final configuration of UR5 manipulators. Note that we only give the command to the first three joints starting from the base joint for this work.

a metric [7], [8]. The Riemannian metric in this context represents the kinetic energy as a function of the system velocity. Previous works [9], [10] have derived optimal control equations using the Pontryagin Maximum Principle under acceleration- or torque-based costs. These approaches focus on minimizing the magnitude of accelerations on inertially defined Riemannian manifolds. Additionally, the influence of potential fields on optimal control equations has been considered through the Riemannian Hessian of the potential field [11], [12].

Similarly, drag-dominated mechanical systems are associated with a Riemannian manifold equipped with a drag metric tensor [13], [5]. This drag metric tensor represents the drag coefficients at each configuration and describes the power dissipated by configuration velocities. In such systems, geodesics on drag manifolds represent the solutions to optimal control problems, as these geodesics find the shortest path and constant-speed profile on the drag manifolds. However, little work has been done on the geometric understanding of optimal trajectories considering the combined effects of kinetic, drag, and gravitational forces beyond these two extreme cases.

In this paper, we aim to provide a geometric understanding of optimal trajectories considering the influence of various

factors and derive an optimal control equation with a general force expressed as a function of configuration and velocity. As illustrated in Fig. 1, we identify three key elements affecting optimal trajectories:

- 1) Inertial Effect: Optimal trajectories are influenced by the curvature of the inertia manifolds. Generally, positive curvature tends to make optimal trajectories converge at specific points [10]. To minimize acceleration- or torque-norm costs, the trajectory on the positive curvature of manifolds generates the acceleration in the direction pointing inward.
- 2) Potential Force Effect: Similar to the inertial effect, optimal trajectories are affected by the curvature of potential manifolds, which are associated with the inertia manifolds [11], [12]. These manifolds are essentially the graphs of potential energy plotted on the inertia manifolds.
- 3) Resistive Force Effect: This effect tends to align optimal trajectories with the drag manifolds. To minimize energy dissipation due to resistive forces, such as joint friction or end-effector drag, it is preferable to follow the shortest path on drag manifolds [5].

To demonstrate our approach and provide a geometric understanding, we apply the optimal control equation to two-link robotic manipulators with rigid bodies and the UR5 manipulator, considering each effect separately in section IV and combining effect in section V. The two-link robotic manipulator, defined by two joint variables, is particularly useful for illustrating the associated manifolds, such as potential fields and drag manifolds. The UR5 is a widely used 6-DOF robotic manipulator in research and industrial applications [14]. In this robot, the first three joints control the position of the end-effector, while the last three joints control its orientation. To highlight the effects of inertia and gravity, we focus on the optimal trajectories within the reduced configuration space defined by the first three joints.

II. BACKGROUND

A. Riemannian geometry

In this section, we briefly review *Riemannian Geometry* from the perspective of optimal control problems and mechanical systems. The detailed formulations or definitions of notions can be found in [15].

A Riemannian *metric* M for the space contains the distance information, and a manifold Q equipped with a metric tensor M is called a *Riemannian manifold* (Q, M) . Let $U \in \mathbb{R}^d$ be an open subset with coordinates $q = (q^1, \dots, q^d)$. U is a coordinate domain in a configuration manifold Q , and it allows to express explicit coordinate formulas for the tensors. $(\partial_{q^i} \equiv \frac{\partial}{\partial q^i})$ denotes the basis of TU given by (constant) vector fields in U and (∂q^i) the dual basis of T^*U .

A (tangent) vector on a manifold describes the rate at which a point moves through a Riemannian manifold Q . A covector describes the rate where a quantity changes across a space at a given point. A covector has a natural product with a tangent vector because it acts as a linear map from tangent

vectors to scalars. It is called a covector-vector product,

$$\frac{dW}{dt} = \langle F; \dot{q} \rangle = \sum_i F_i \dot{q}^i, \quad (1)$$

where $\langle \cdot; \cdot \rangle$ denotes a covector-vector product, $F \in T_q^*Q$ is a covector, $\dot{q} \in T_qQ$ is a configuration velocity, and W is a corresponding scalar quantity. From the viewpoint of mechanics, force fields F can be interpreted as covector fields, and velocity fields \dot{q} can be interpreted as vector fields. Then, a covector-vector product between forces and velocities calculates the time-derivative of work scalars (i.e., power).²

There is a natural isomorphism between the cotangent and tangent bundles of Riemannian manifolds via the metric M :

$$\langle F, \bullet \rangle_{M^*} = M^{ij} F_j \partial_{q^i} = a, \quad (2a)$$

$$\langle a, \bullet \rangle_M = M_{ij} a^i \partial q^j = F, \quad (2b)$$

where $\langle \cdot, \cdot \rangle_M$ is the inner product with respect to M , $F \in T_q^*Q$ is a covector, $a \in T_qQ$ is a tangent vector, and M_{ij} , the bullet notations \bullet represent an element of T_qQ or T_q^*Q so that the corresponding linear function is a dual element in T_q^*Q or T_qQ , and M^{ij} are the components of M and its inverse (i.e., dual), respectively. The operations in (2a) and (2b) raise and lower vector indices, transforming between vectors and covectors.³ From the viewpoint of mechanics, raising the index transforms a force covector into an acceleration vector through the mass matrix $M(q)$.

Unlike a flat space, the local coordinate bases of a curved space can vary at each point. A covariant derivative is a coordinate-invariant way to differentiate tensor (e.g., vector or covector) fields along curves by including correction terms for changes in the local coordinate bases. A covariant derivative of a vector $\nabla_{\dot{q}} \dot{q}$ and a covector $\nabla_{\dot{q}}^* F$ along the curve $q(t)$ can be expressed in natural coordinates induced by coordinates (q^i) in Q :

$$(\nabla_{\dot{q}} \dot{q})^i = \ddot{q}^i + \Gamma_{jk}^i \dot{q}^j \dot{q}^k, \quad (3)$$

$$(\nabla_{\dot{q}}^* F)_i = \dot{F}_i - \Gamma_{ij}^k F_k \dot{q}^j, \quad (4)$$

where $\dot{q}(t)$ is a time-parameterized curve, ∇ and ∇^* are the Levi-Civita Connection corresponding to a metric M and its dual connection, Γ_{jk}^i is Christoffel symbols [15]. A *covariant acceleration* $\nabla_{\dot{q}} \dot{q}$ is a time-covariant derivative of a velocity \dot{q} along a curve $q(t)$. If a covariant acceleration is zero, $q(t)$ is called a *geodesic*.

A Riemannian curvature tensor $R \in \Omega^2(Q, \text{End}(TQ))$ describes a curvature of the curvature of Riemannian manifolds and is defined by a commutator of a covariant derivative,

$$R(X, Y)Z = \nabla_X \nabla_Y Z - \nabla_Y \nabla_X Z - \nabla_{[X, Y]} Z, \quad (5)$$

²We use an Einstein summation convention. A lower index indicates covector elements and an upper index indicates vector elements.

³These operations are known as a musical isomorphism operator. For raising an index, a musical sharp symbol is used ($a = F^\sharp$). For lowering an index, a musical flat symbol is used ($F = a^\flat$).

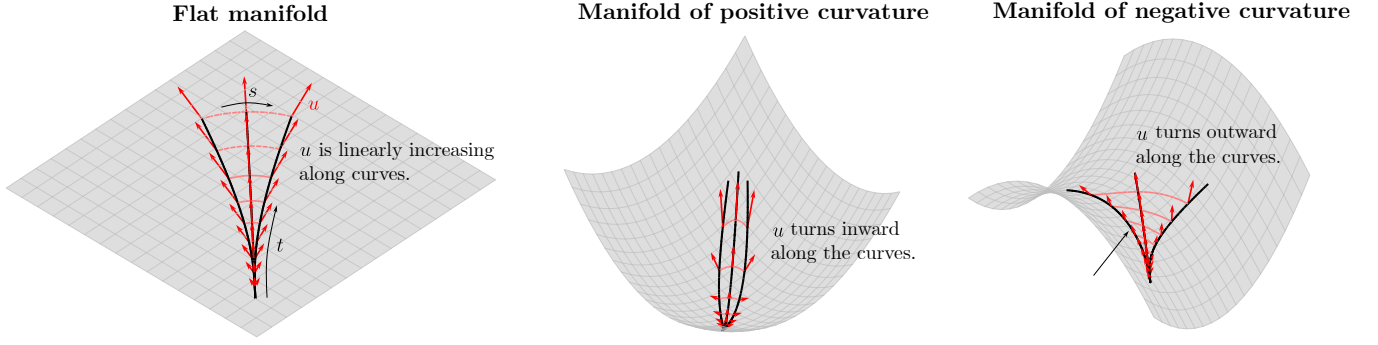


Fig. 2. A one-parameter family of optimal trajectories in inertia manifolds of different curvatures. s is a variation parameter. t is a time parameter of each curve. The vector field u is a control input. Black curves denote one of the optimal trajectories in the family. (a) Optimal trajectories families in flat manifolds. Because of the zero curvature, the optimal trajectory is a fourth-order polynomial spline equation [10]. (b) Optimal trajectories families in manifolds of positive curvature (e.g., spherical type of manifolds). Because of positive curvature, a direction of control inputs u is gradually turning inward. (c) Optimal trajectories families in manifolds of negative curvature (e.g., saddle type of manifolds). Because of positive curvature, a direction of control inputs u is gradually turning outward.

where $[\cdot, \cdot]$ is a Lie bracket on Q , and R is a (3,1)-type tensor field. Its coefficient function $R_{ijk}^l(q)$ is defined by

$$\begin{aligned} \langle \partial q^l, R(\partial_{q^i}, \partial_{q^j}) \partial_{q^k} \rangle &= R_{ijk}^l(q) \\ &= \partial_{q^i} \Gamma_{jk}^l - \partial_{q^j} \Gamma_{ik}^l + \Gamma_{jk}^n \Gamma_{in}^l - \Gamma_{ik}^n \Gamma_{jn}^l, \end{aligned} \quad (6)$$

III. OPTIMAL CONTROL PROBLEM

A. Optimal Control System

The optimal control system is defined by the data $(Q, M, N, a_{\text{ext}})$, where Q is configuration manifold, M is a “mass” metric, N is an induced metric encoding control cost [10], and $a_{\text{ext}} = \langle F_{\text{ext}}, \bullet \rangle_{M^*}$ is an equivalent acceleration field generated by an external force F_{ext} dependent on configuration and velocity, including gravitational⁴ and drag forces.

The system is given by:

$$\text{State: } x(t) = (q(t), \dot{q}(t)) \in TQ, \quad (7a)$$

$$\text{Control: } \nabla_{\dot{q}} \dot{q} = u + a_{\text{ext}}(q, \dot{q}), \quad (7b)$$

$$\text{Cost: } \int_0^T \|u\|_N^2 dt, \quad (7c)$$

$$\text{Initial Condition: } q(0) = q_0, \quad \dot{q}(0) = v_0, \quad (7d)$$

$$\text{Final Condition: } q(T) = q_T, \quad \dot{q}(T) = v_T, \quad (7e)$$

where u is a control input, and T is a trajectory time. Raising an index in the control equation gives the Euler-Lagrange equation,

$$M(q)\ddot{q} + C(q, \dot{q}) = M(q)u + F_{\text{ext}}(q, \dot{q}), \quad (8)$$

where $C(q, \dot{q})$ represents centrifugal and Coriolis forces, interpretable as Christoffel symbols. We use an acceleration-based input norm with respect to N for the cost functional. Based on the induced metric, a cost functional has a different meaning. For example, the actuator-torque norm cost can be defined by

$$N = M^T \tilde{M} M, \quad \|u\|_N^2 = \|F\|_{\tilde{M}}^2, \quad (9)$$

⁴Although a Lagrangian includes potential energy, we interpret a gravitational force as an external force to “inertia manifold” in this paper.

with \tilde{M} being the torque-based cometric tensor, which reduces to the Euclidean metric when joint and actuator configurations are identical [10].

B. Optimal Spline Equation

To get a system of equations that determine the optimal trajectory $q(t) \in Q$ in this setting, we shall use the Pontryagin Maximum Principle (PMP).⁵

Following [9], [10], using the Levi-Civita connection $\nabla \equiv \nabla^M$, the Hamiltonian system (P, Ω, H) coming from PMP has phase space isomorphic to

$$\begin{aligned} H = T^*Q \times_Q TQ \times_Q T^*Q, \quad \Omega = \omega_{\nabla}, \\ \text{with variables } p, \alpha \in T_q^*Q, v \in T_qQ, \end{aligned} \quad (10)$$

where ω_{∇} is isomorphic to the canonical symplectic form under a diffeomorphism $P \simeq T^*(TQ)$ (see [9]). The Hamiltonian $H = \max_u(H_u)$ comes from the family

$$H_u = -\|u\|_N^2 + \langle p, v \rangle + \langle \alpha, u + a_{\text{ext}} \rangle, \quad (11)$$

leading to

$$H = \frac{1}{4} \|\alpha\|_{N^*}^2 + \langle \alpha, a_{\text{ext}} \rangle + \langle p, v \rangle, \quad u_{\text{max}} = \frac{1}{2} N^* \alpha. \quad (12)$$

Using the formulas for ω_{∇} and the corresponding Hamiltonian vector fields in [9, Prop. 1], we arrive at the following system of equations written in natural coordinates induced by coordinates (q^i) in Q ,

Proposition 1. *The optimal trajectory $q(t) \in Q$ for the control system defined by the data $(Q, M, N, a_{\text{ext}})$ as above, is given by a solution of the following Hamiltonian system: for unknowns $q(t) \in Q$, $p(t), \alpha(t) \in T_{q(t)}^*Q$ and $\dot{q}(t) \in$*

⁵Alternatively, one can look directly for critical points of the cost L .

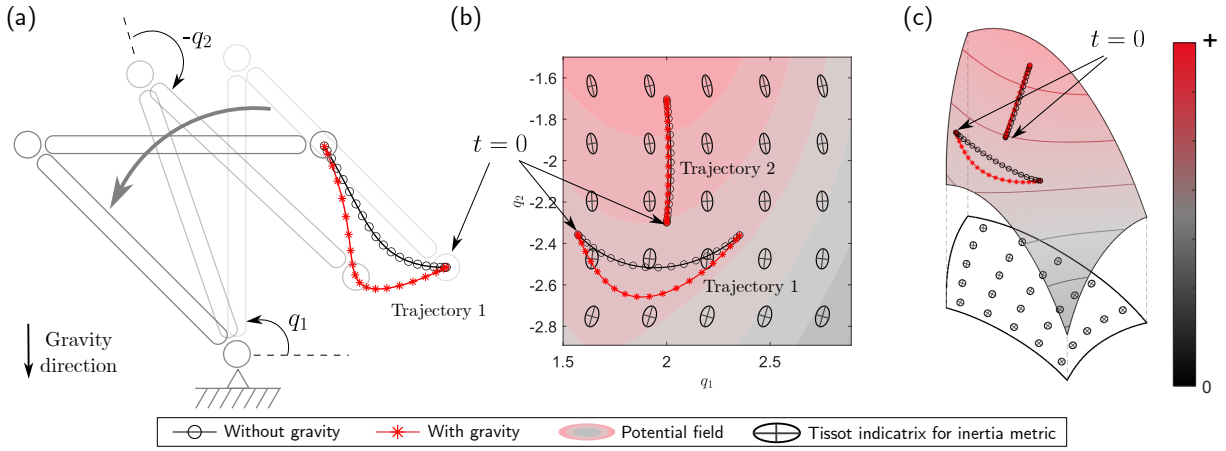


Fig. 3. (a) A two-link manipulator and optimal trajectories under situations with and without gravitation force in task space. The mass and the length of each link are the same (m, ℓ). q_i is a joint angle of i -th link and a configuration. The direction of gravity force is toward the bottom. (b) The same optimal trajectories in configuration space. The potential field is visualized via a filled contour. The inertia metric is visualized by their Tissot's indicatrix (ellipse and cross lines) which describes how much the space shrinks or expands at each point in a geometric viewpoint or how much velocity is needed at each point to produce unit kinetic energy in a mechanics viewpoint. (c) Optimal trajectories on a potential field with a metric-stretched space. The metric-stretched space approximates the geometry of the manifold such that basis vectors in each direction at each point correspond to the same kinetic energy as much as possible. This algorithm is presented in [16]. The blue- and black-colored curves respectively are the optimal trajectories generated by the optimal control of the two-link manipulator with and without gravity. In this space, the Tissot indicatrix ellipses have a circular-like shape. A surface at the top visualizes the potential field. The normal distance between the stretched surface and each point on the potential field surface represents potential energy at each configuration. We use the same colormap of a filled contour as that of (b).

$$\begin{aligned}
 & T_{q(t)}Q, \\
 & \dot{q}^i = v^i, \\
 & (\nabla_v v)^i = \frac{1}{2} N^{ij} \alpha_j + a_{ext}^i, \\
 & (\nabla_v^* \alpha)_i = -p_i - \alpha_j (\partial_{v^i} a_{ext}^j), \\
 & (\nabla_v^* p)_i = -\frac{1}{4} \tau_i^{jk} \alpha_j \alpha_k + R_{ijk}^l v_j v_k \alpha_l \\
 & \quad - \underbrace{[\alpha_k (\nabla_{\partial_{q^i}} a_{ext})^k - \Gamma_{ij}^k v^j (\partial_{v^k} a_{ext}^l) \alpha_l]}_{\text{External force terms}}, \quad (13)
 \end{aligned}$$

where, as in [10, Appendix A], R and ∇ are associated with a metric tensor M , and the tensor $\tau_i^{jk} \equiv \nabla_v^* N^*$ is given by a covariant derivative of a dual induced tensor,

$$\tau_i^{jk}(q) = \partial_{q^i} N^{jk} + \Gamma_{il}^j N^{lk} + \Gamma_{il}^k N^{jl}. \quad (14)$$

We skip the coordinate-invariant version of the equations for the purpose of this paper. The coordinate-invariant approach will be discussed elsewhere.

IV. GEOMETRIC INTUITION

In this section, we describe the geometric meaning of the optimal spline equation. Even though the optimal control equation in (13) is general for the external force, we narrow down the scope for our interest in the gravitational and drag forces. We consider a simple model for a resistive force and include a potential force,

$$F_{ext} = -d\mathcal{V} - D(q)\dot{q}, \quad (15)$$

where D is a drag tensor containing information about the drag coefficient for each direction with respect to a configuration, $\mathcal{V} : Q \rightarrow \mathbb{R}$ is the potential energy as a smooth

function of a configuration (i.e., a smooth scalar field) on a configuration manifold Q , and $d\mathcal{V}$ is an Euclidean gradient of potential energy. With this setting, the optimal control system of interest is defined by the data $(Q, M, N, a_{ext}) \equiv (Q, M, N, \mathcal{V}, D)$.

For a straightforward explanation through this section, we consider the acceleration-based norm cost, which makes the dual inertia metric the cometric so that the data we consider is reduced to (Q, M, \mathcal{V}, D) ,

$$N = M \text{ and } \|u\|_N^2 = \|u\|_M^2 \quad (16)$$

A. Inertial effect

Consider Without the external force and with the acceleration-based cost, the optimal spline equation in (13) reduces to a Riemannian spline equation governed by the Riemannian curvature tensor term,

$$\nabla_v^2 u + R(u, v)v = 0. \quad (17)$$

The Riemannian spline equation resembles the geodesic variation (Jacobi) equation [15], allowing for a similar geometric interpretation. On flat manifolds with zero curvature, as illustrated in Fig. 2(a), control input u increases or decreases linearly along the trajectory. On manifolds of positive curvature, geodesics tend to converge, and the Riemannian curvature term, as illustrated in Fig. 2(b), causes control inputs to point inward, leading to trajectory convergence. Conversely, on manifolds of negative curvature, control inputs point outward, resulting in trajectory divergence, as illustrated in Fig. 2(c).

B. Potential force

Consider a conservative dynamical system, which means that the external force only includes a potential force. The

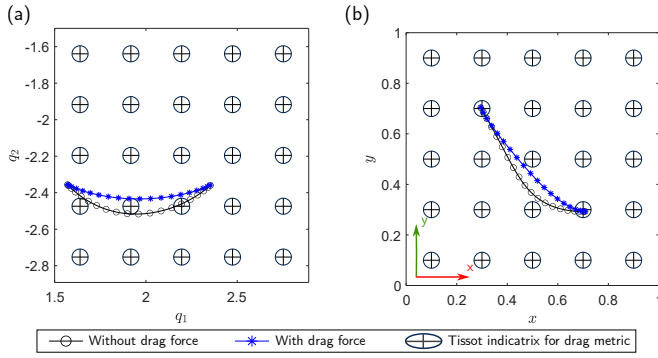


Fig. 4. (a) Optimal trajectories of a two-link manipulator with and without joint friction. The black and blue curves represent the trajectories without and with friction, respectively. In configuration space, joint friction follows an Euclidean metric, resulting in circular-shape Tissot indicatrices. The trajectory with friction is closer to a straight path. (b) Optimal trajectories of the same manipulator with an end-effector drag force. The black and blue curves represent trajectories without and with drag. In task space, drag follows an Euclidean metric, yielding circular-shape Tissot indicatrices. The trajectory with drag is closer to a straight path.

equivalent acceleration generated by the potential force is a Riemannian gradient of potential energy with respect to an inertia metric M : $\text{grad} \equiv \text{grad}_M$ [15],

$$-\text{grad}(\mathcal{V}) = -\langle d\mathcal{V}, \bullet \rangle_{M^*} = a_{\text{ext}}. \quad (18)$$

A Riemannian Hessian of a scalar field (e.g., a potential field) associated with an inertia metric M describes a second-order effect of a function on the manifold: $\text{Hess} \equiv \text{Hess}_M$ [15],

$$\text{Hess}(\mathcal{V})(X, Y) = \langle \nabla_X \text{grad}(\mathcal{V}), Y \rangle_M. \quad (19)$$

A Riemannian Hessian of a potential field describes the local curvature of a function with respect to tangent vectors on Riemannian manifolds.

The potential force term in (13) reduces to an inner product of the acceleration-based control input u and a Riemannian gradient of potential energy. By the definition of Riemannian Hessian, this term is equivalent to a Riemannian Hessian of potential energy,

$$-2 \langle \alpha; \nabla_{\bullet} a_{\text{ext}} \rangle = \langle \nabla_{\bullet} \text{grad}(\mathcal{V}), u \rangle_M = \text{Hess}(\mathcal{V})(\bullet, u), \quad (20)$$

The potential energy term in optimal spline equation (13) is equivalent to the vector contracting potential Hessian with a control input u . Because of the sign difference from the definition of the potential force, a positive local curvature of potential fields makes the control input points outward. From the viewpoint of mechanics, the controller uses the gravity force to reduce the use of the control input as much as possible. Thus, the optimal trajectory prefers the route where the control input aligns with the direction changing in a potential force and avoids the misaligned direction.

Examples: As illustrated in Fig. 3, we compare two optimal trajectories for a two-link manipulator with and without gravity to evaluate its effect. The inertia tensor is derived by pulling back each link's individual inertia tensor through its Jacobian. A detailed derivation of a mass matrix and a

potential field can be found in [17], [18]. For this example, we use a torque norm as the cost functional, with a torque-based cometric tensor that reduces to the identity matrix due to its physical configurations. Two scenarios of optimal control are considered. The initial and final configuration conditions of each scenario are

$$1) q_0 = \left[\frac{1}{2}\pi \quad -\frac{3}{4}\pi \right]^T, \quad q_T = \left[\frac{3}{4}\pi \quad -\frac{3}{4}\pi \right]^T, \quad (21a)$$

$$2) q_0 = [2 \quad -2.3]^T, \quad q_T = [2 \quad -1.7]^T. \quad (21b)$$

The initial and final velocity conditions of both scenarios are zero velocities.

Roughly speaking, the left-upper region of the potential field in Fig. 3(b) has a positive curvature, and the left-lower region has a negative curvature. Thus, optimal trajectories under the gravity effect are more distorted toward the negative curvature of the potential field than those without the gravity effect. Especially, if we set the initial and final conditions so that the optimal trajectories are aligned with the direction of a curvature effect (e.g., a vertical trajectory in Fig. 3(b)), a phase and an end time of trajectories with a gravity effect are different with those without a gravity effect.

C. Resistive Force

Unlike a potential force, a resistive force such as friction or drag force dissipates energy in mechanical systems. Thus, we can expect a trajectory with a short path length under the drag geometry to be advantageous. In other words, adding the drag effect to the optimal control would make the shape of an optimal trajectory closer to a geodesic shape on the drag manifold.

With a drag effect, a trajectory minimizing a cost is affected by three different terms,

$$\|u\|_N^2 = \|\nabla_v v\|_N^2 + \|v\|_{D'}^2 + 2 \langle \langle \nabla_v v, \bullet \rangle_M, \langle v, \bullet \rangle_{\tilde{M}} \rangle, \quad (22)$$

where an induced drag metric tensor $D' = D^T \tilde{M} D$ encodes the anti-dual of a cometric tensor with respect to a drag tensor. The first term is the covariant acceleration norm, dominated by an inertia manifold. The second term can be interpreted as the drag force norm associated with the inertia metric or the velocity norm on the manifold associated with an induced drag metric tensor. To minimize the integral of the velocity norm along the trajectory, a short pathlength on the drag manifold and constant-speed profile is desirable due to this term [13], [19]. The third term is the coupling effect represented by the inner product of inertia and drag forces with respect to the cometric tensor. Without a drag effect, the second and third terms vanish.

Examples: As illustrated in Fig. 4, we apply optimal control to achieve four different scenarios of optimal trajectories for a two-link manipulator with and without two types of drag force: 1) a joint friction and 2) a drag force applying to the end-effector. We assume that the drag coefficient is the same in each direction and use a viscous friction model for simplicity. The joint friction tensor is identical to the Euclidean metric. The end-effector drag tensor can be

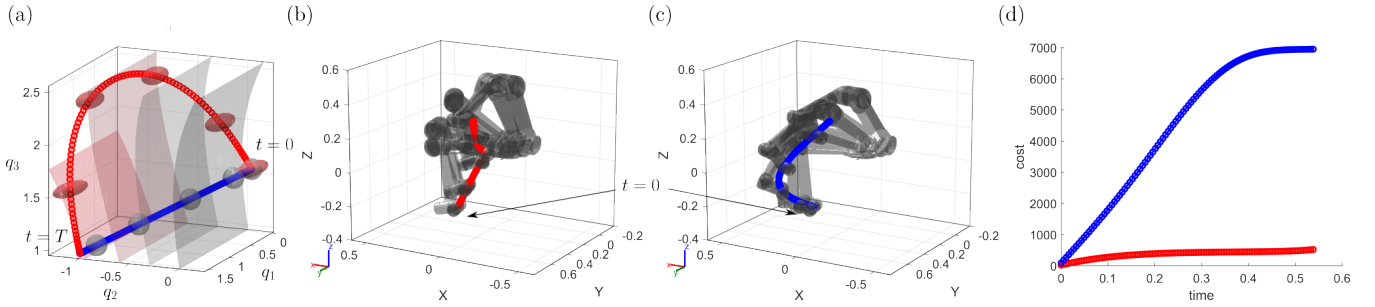


Fig. 5. (a) Optimal trajectories for a UR5 moving its first three joints under the combinational effect of inertia, gravitation, and drag force. Tissot indicatrices visualize the metric space at given points of the trajectory. The red-colored curve denotes an optimal trajectory under the torque-based cometric. The blue-colored curve denotes an optimal trajectory under the Euclidean metric, and it is the same as the interpolation results between initial and final conditions. The set of surfaces denotes a level set of a potential field. (b) An optimal trajectory of UR5 manipulator under the torque-based cometric in task space. (c) An optimal trajectory of UR5 manipulator under the Euclidean metric or a trajectory interpolated between initial and final conditions in task space. (d) A time versus a torque norm cost. A cost can be derived by the time-integral of a torque norm.

constructed by pulling back the inertia tensor of the end link through the kinematic Jacobian. A detailed derivation of a drag tensor can be found in [5]. We considered the same as the first scenario in (21).

Fig. 4(a) illustrates the comparison between the trajectory with and without the joint friction. The optimal trajectory without joint friction is distorted because of the curvature effect of the inertia manifolds. On the other hand, the optimal trajectory with joint friction is distorted by combining the curvature effect with the straightening effect of the drag manifold. Fig. 4(b) illustrates the comparison between the trajectory with and without the drag force applied to the end-effector. In task space, the drag coefficient in each direction is identical. Similarly, the optimal trajectory with an end-tip drag force is more straight than the optimal trajectory without an end-tip drag force.

V. RESULTS

We applied the methods in (13) to construct an optimal control scheme for a UR5 manipulator. The initial and final configuration conditions are $q_0 = [0.1, 0.1, \pi/2]^T$, $q_T = [\pi/2, -1, 1]^T$ and fixed the remaining joint values as 0.1. The initial and final velocity conditions are zero velocities. Note that we only give the command to the first three joints starting from the base joint to decrease computational cost and visualize the trajectory, even though the method can be applied to high-dimensional systems. The dynamical system of UR5 includes the gravity and joint friction forces. The mass and linkage length information can be found in [14]. We assume a viscous friction model for simplicity. To visualize the robots, we use MATLAB's Robotics System Toolbox. To solve the boundary value problems in this paper, we use the multiple shooting method based on the CasADi's automatic differentiation [20].

As illustrated in Fig. 5, we compare two optimal trajectories for the UR5 manipulator under the same initial and final conditions, accounting for joint friction and gravitational effects. The Euclidean metric trajectory interpolates between the start and end states, while the torque-based cometric trajectory accounts for inertia, resulting in a path that may

appear longer in joint space but is more efficient. Fig. 5(b-c) illustrates the differences between the torque-optimal and Euclidean metric trajectories in task space. The torque-optimal trajectory initially folds the arm to minimize inertia effects and then stretches it to reach the final configuration, where inertia has less impact. As illustrated in Fig. 5(d), the cost of the torque-optimal trajectory increases moderately over time compared to the Euclidean metric trajectory and represents a more efficient route overall so that the control input (or the trajectory) aligns with the shorter axis of the Tissot ellipsoids.

VI. CONCLUSIONS

In this paper, we have presented a geometric framework for understanding optimal control in mechanical systems, considering the effects of inertia and external forces (e.g., drag and gravitational forces). By employing Riemannian geometry to describe these systems, we gained insights into how these external forces influence optimal trajectories. We derived the optimal control equations based on the Pontryagin Maximum Principle and demonstrated their application to two-link and UR5 robotic manipulators, highlighting the curvature effects of each manifold and the path-shortening influence of resistive forces. This approach not only enhances our understanding of trajectory optimization but also provides a foundation for applying geometric optimal control methods to a wide range of robotic systems (e.g., locomoting systems [21], [22]) and mechanical applications. Future work could explore the integration of additional forces and constraints (e.g., nonholonomic constraints [23]), further broadening the applicability of this geometric approach to more complex systems.

ACKNOWLEDGMENT

We acknowledge the support in part by the Office of Naval Research under awards N00014-23-1-2171 and the Brazilian agency grants CNPq 309847/2021-4, 402320/2023-9 and FAPERJ JCNE E-26/203.262/2017.

REFERENCES

- [1] P. M. Wensing, M. Posa, Y. Hu, A. Escande, N. Mansard, and A. D. Prete, "Optimization-Based Control for Dynamic Legged Robots," *IEEE Transactions on Robotics*, vol. 40, pp. 43–63, 2024.
- [2] W. Xi and C. D. Remy, "Optimal gaits and motions for legged robots," in *2014 IEEE/RSJ International Conference on Intelligent Robots and Systems*, pp. 3259–3265, Sept. 2014. ISSN: 2153-0866.
- [3] Y.-M. Chen, J. Hu, and M. Posa, "Beyond Inverted Pendulums: Task-Optimal Simple Models of Legged Locomotion," *IEEE Transactions on Robotics*, vol. 40, pp. 2582–2601, 2024. Conference Name: IEEE Transactions on Robotics.
- [4] J. Choi and R. L. Hatton, "Optimal Control Approach for Gait Transition with Riemannian Splines," Sept. 2024. arXiv:2409.09224 [cs].
- [5] S. Ramasamy and R. L. Hatton, "The Geometry of Optimal Gaits for Drag-Dominated Kinematic Systems," *IEEE Transactions on Robotics*, vol. 35, pp. 1014–1033, Aug. 2019. Number: 4.
- [6] S. Kadam, K. S. Phogat, R. N. Banavar, and D. Chatterjee, "Exact Isoholonomic Motion of the Planar Purcell's Swimmer," *IEEE Transactions on Automatic Control*, vol. 67, pp. 429–435, Jan. 2022. Number: 1.
- [7] A. M. Bloch, *Nonholonomic mechanics and control*. No. 24 in Interdisciplinary applied mathematics, New York: Springer, 2010.
- [8] F. Bullo and A. D. Lewis, *Geometric Control of Mechanical Systems: Modeling, Analysis, and Design for Simple Mechanical Control Systems*, vol. 49 of *Texts in Applied Mathematics*. New York, NY: Springer, 2005.
- [9] P. Balseiro, A. Cabrera, T. J. Stuchi, and J. Koiller, "About simple variational splines from the Hamiltonian viewpoint," *Journal of Geometric Mechanics*, vol. 9, no. 3, pp. 257–290, 2017. Number: 3 arXiv:1711.02773 [math].
- [10] A. Cabrera and R. L. Hatton, "Optimal control of robotic systems and biased Riemannian splines," *ESAIM: Control, Optimisation and Calculus of Variations*, vol. 30, p. 36, 2024. Publisher: EDP Sciences.
- [11] I. Hussein and A. Bloch, "Optimal control on Riemannian manifolds with potential fields," in *2004 IEEE Conference on Decision and Control (CDC)*, pp. 1812–1817 Vol.2, IEEE, 2004.
- [12] F. Dubois, D. Fortuné, J. A. Rojas Quintero, and C. Vallée, "Pontryagin Calculus in Riemannian Geometry," in *Geometric Science of Information* (F. Nielsen and F. Barbaresco, eds.), vol. 9389, pp. 541–549, Cham: Springer International Publishing, 2015.
- [13] S. D. Kelly and R. M. Murray, "Geometric phases and robotic locomotion," *Journal of Robotic Systems*, vol. 12, no. 6, pp. 417–431, 1995. Number: 6 eprint: <https://onlinelibrary.wiley.com/doi/pdf/10.1002/rob.4620120607>.
- [14] P. M. Kebria, S. Al-wais, H. Abdi, and S. Nahavandi, "Kinematic and dynamic modelling of UR5 manipulator," in *2016 IEEE International Conference on Systems, Man, and Cybernetics (SMC)*, pp. 004229–004234, Oct. 2016.
- [15] J. M. Lee, *Riemannian manifolds: an introduction to curvature*. No. 176 in Graduate texts in mathematics, New York Berlin Heidelberg: Springer, nachdr. ed., 1997.
- [16] R. L. Hatton, T. Dear, and H. Choset, "Kinematic Cartography and the Efficiency of Viscous Swimming," *IEEE Transactions on Robotics*, vol. 33, pp. 523–535, June 2017. Number: 3.
- [17] K. M. Lynch and F. C. Park, *Modern robotics: mechanics, planning, and control*. Cambridge: Cambridge university press, 2017.
- [18] R. L. Hatton, Z. Brock, S. Chen, H. Choset, H. Faraji, R. Fu, N. Justus, and S. Ramasamy, "The Geometry of Optimal Gaits for Inertia-Dominated Kinematic Systems," *IEEE Transactions on Robotics*, vol. 38, pp. 3279–3299, Oct. 2022. Number: 5 Conference Name: IEEE Transactions on Robotics.
- [19] S. Ramasamy, *Geometry of Locomotion*. PhD thesis, Oregon State University, Aug. 2020.
- [20] J. A. E. Andersson, J. Gillis, G. Horn, J. B. Rawlings, and M. Diehl, "CasADi: a software framework for nonlinear optimization and optimal control," *Mathematical Programming Computation*, vol. 11, pp. 1–36, Mar. 2019.
- [21] J. Choi, C. Bass, and R. L. Hatton, "Optimal Gait Families using Lagrange Multiplier Method," in *2022 IEEE/RSJ International Conference on Intelligent Robots and Systems (IROS)*, pp. 8873–8878, Oct. 2022. ISSN: 2153-0866.
- [22] Y. Yang and R. L. Hatton, "Geometric Gait Optimization for Inertia-Dominated Systems with Nonzero Net Momentum," in *2023 IEEE/RSJ International Conference on Intelligent Robots and Systems (IROS)*, (Detroit, MI, USA), pp. 2877–2884, IEEE, Oct. 2023.
- [23] I. I. Hussein and A. M. Bloch, "Optimal Control of Underactuated Nonholonomic Mechanical Systems," *IEEE Transactions on Automatic Control*, vol. 53, pp. 668–682, Apr. 2008. Conference Name: IEEE Transactions on Automatic Control.